JACS
JOURNAL OF THE AMERICAN CHEMICAL SOCIETY

Article

pubs.acs.org/JACS

Fully Hydrogenated Beryllium Nanoclusters

Emmanuel N. Koukaras,*[,†] Aris P. Sgouros,[‡,§] and Michael M. Sigalas[§]

[†]Nanotechnology and Advanced Materials Laboratory, Department of Chemical Engineering, University of Patras, 26500 GR Patras, Greece

[‡]School of Chemical Engineering, National Technical University of Athens (NTUA), GR-15780 Athens, Greece

[§]Department of Materials Science, University of Patras, GR-26504 Patras, Greece

Supporting Information

ABSTRACT: We present the ground state and energetically low structures of Be_nH_{2n} nanoclusters as predicted using density functional theory (DFT) and employing the M06 meta-hybrid exchange-correlation functional. Results using the M06 functional are benchmarked against high accuracy coupled-cluster CCSD(T) and found to be in excellent agreement. For small values of n, the linear or polymeric form is the lowest energy geometry, while for sizes larger, $n > 9$ ring type and link type structures are the energetically lowest configurations. This trend has also been observed through ab initio molecular dynamics (AIMD) simulations at finite temperatures. In addition to the binding energies of the structures we report on polymerization energies, Be−H bond energies with respect to coordination details, hydrogen desorption energies of saturated and oversaturated species, as well as computed infrared spectra of all the ground state and energetically low lying structures presented. Furthermore, we find that the saturated polymeric forms of the nanoclusters *cannot* retain molecular hydrogen, in contrast to what is expected when zero point energy corrections are not taken into account.

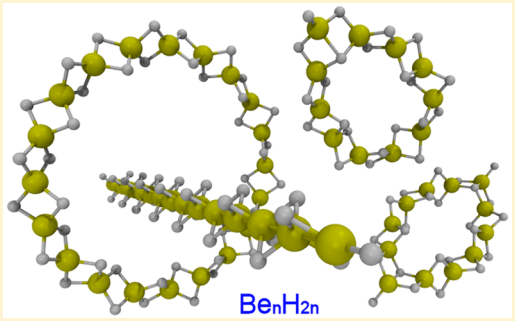

INTRODUCTION

The structural conformations and properties of nanoparticles (NPs) may differ significantly from their bulk counterparts. Factors that contribute to such differences may be induced by structural strains or change in reactivity, due to large surface to volume ratios at the nanoscale, or changes of energy levels due to quantum confinement.[1−4] In this respect, metal-hydride nanoparticles have been recently suggested as being more efficient for hydrogen storage compared to their corresponding bulk materials.[3,5−7] This motivated research in metal hydride NPs for applications in hydrogen storage, such as beryllium hydride which in bulk and nanostructure form has been studied for hydrogen storage since it has the highest hydrogen weight percentage (18.2 wt % H_2),[5,8,9] and hydrogen desorption temperature at moderately high levels, about 250 °C.[5] Despite the advantages of BeH_2 there are toxicity issues[5] that make its hydrogen storage applications unattractive. Beryllium hydride exhibits differences between scales, with NPs being of polymeric[10−12] and ring type forms as shown in Figure 1, while the crystal structure of bulk BeH_2 has a body centered orthorhombic unit cell corresponding to the *Ibam* or *Iba*2 space groups.[13] Also in this respect, in studying beryllium hydride at its smallest scale (BeH_2 molecule) Mo et al. have recently shown[14] that significant mutual interactions manifest between beryllium bonds and hydrogen bonds when both types of interactions are present in the same molecular system. This has far reaching consequences, with beryllium bonds competing or even replacing hydrogen bonds, and also dramatically affect the strength of intramolecular hydrogen bonds of the interacting species.

Interest in beryllium and it is hydrides and oxides has been recently renewed in light of its use in the international thermonuclear experimental reactor (ITER) as a plasma-facing (first wall) armoring material.[15−17] In this case, safety concerns arise from possible release of chemical toxic substances in the event of accidents (for modeling of accidental release source terms), and focus is on beryllium dust characterization, resuspension and filtration.[15,16] A better understanding of the properties of these NPs should greatly enhance the efficiency of the methods employed, which to date are largely empirical.[15]

While our initial interest in such systems[3,7] was with respect to hydrogen storage applications, we later opted to examine structural properties and energies of these NPs to extend the fundamental understanding of the systems and their properties. In the present study, DFT calculations were performed, in combination with high accuracy coupled cluster theory calculations, to explore the appearance of ring structures in Be_nH_{2n} nanoparticles. There were already indications of the appearance of ring like structures in Be_nH_{2n} NPs from a previous study.[7] From the calculations, it is evident that ring structures are energetically more favorable above a certain value of n. We also examine the possibility of absorbing hydrogen atoms beyond the Be_nH_{2n} stoichiometric percentage, for values of n

Received: January 6, 2016
Published: February 23, 2016

DOI: 10.1021/jacs.6b00135
J. Am. Chem. Soc. 2016, 138, 3218−3227

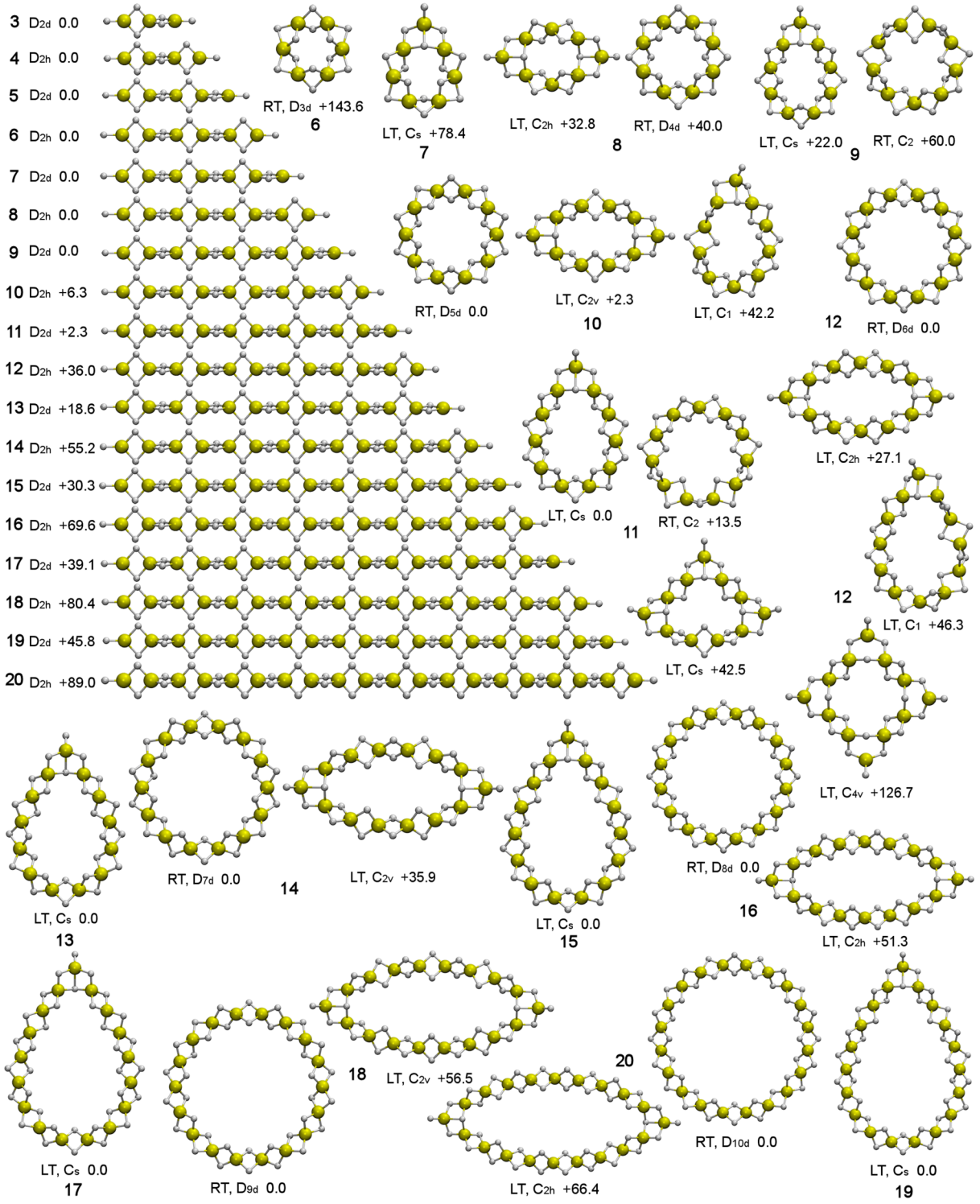

Figure 1. Ground state and energetically low structures of Be_nH_{2n} nanoclusters for n = 3−20. The structures are characterized by their symmetry, by RT for ring type and by LT for link type. Energies of the structures are given relative to (with ZPE corrections) the corresponding ground state structure for a given n, in kJ mol^{-1}.

lower than the ring structure critical number. In such cases the resulting structures would have even higher hydrogen weight percentage than the corresponding bulk value and with different desorption characteristics; thus seemingly providing means for adjustable hydrogen desorption within a wider range of conditions. We show that, upon careful examination, such structures *cannot* retain molecular hydrogen. Computed infrared spectra of all the structures are provided and discussed in comparison to experimentally measured spectra.[10,18]

COMPUTATIONAL TECHNIQUES

The initial geometry optimizations were performed employing density functional theory (DFT) within the generalized gradient approximation (GGA). In particular, the gradient corrected functional of Perdew, Burke and Ernzerhof, PBE[19] was used along with the triple-ζ quality

DOI: 10.1021/jacs.6b00135
J. Am. Chem. Soc. 2016, 138, 3218−3227

basis set def-TZVP.[20] The optimized structures were passed to the second stage of geometry optimizations employing Truhlar's meta-hybrid M06 functional[21] using the cc-pVTZ basis set.[22] Tight convergence criteria were placed for the SCF energy (up to 10^{-8} Eh) and the one-electron density (rms of the density matrix up to 10^{-9}) as well as for the norm of the Cartesian gradient (residual forces both average and maximum smaller than 10^{-6} a.u.). At a final stage, vibrational analysis was performed on all structures to ensure that they are minima of the potential energy hypersurface, i.e., that vibrational modes with imaginary frequencies do not exist. Also, with this stage we obtained the necessary zero point corrections to the energies of the structures. As we shall show, for the systems under study these corrections to the energy have a strong impact on certain energy quantities due to the small energy differences between configurations. Comparisons were made with results from coupled-cluster theory, including singlet and doublet excitations (CCSD), and CCSD(T) which additionally includes triplet excitations noniteratively,[23,24] either performed by us or taken from the literature when available. As we shall discuss in the text and in the Supporting Information, the use of a dense (150,974) grid for integration combined with a (75,302) coupled perturbed Kohn–Sham (CPKS) grid was necessary in order to obtain reliable results. All of the geometry optimizations and energy calculations were performed with the GAUSSIAN package.[25]

We performed ab initio molecular dynamics simulations on the Born–Oppenheimer potential hypersurface as a means to identify possible alternate low energy cluster geometries. Unless otherwise stated the AIMD simulations were performed employing the PBE functional and using the newer def2-TZVPP basis set.[26] In a previous study of beryllium and beryllium hydride nanoparticles and nanocrystals the PBE functional was successfully used to produce structures and obtain binding energies of crystalline Be in good agreement with experiments and at a moderate computational cost compared to the high accuracy methods employed herein. For the temperature control we employed a Nosè–Hoover thermostat[27,28] with an effective relaxation time of 9.7 fs to generate a canonical (NVT) ensemble. The simulations were performed in a vacuum using the leapfrog integration algorithm and a time step of 0.97 fs (40 au). The relaxation time was so chosen for proper equilibration (~2–10 time steps, as suggested by ref 29) within the canonical ensemble. In order to examine whether other nearby local minima configurations exist to the lowest energy configurations that were obtained from DFT calculations (even though this does ensure that a global minimum is found), both the lowest and some higher (up to three) energy configurations from the same cluster of atoms were subjected to high temperature AIMD simulations (from 700 K for the smallest cluster up to 1400 K) and left to relax for up to 20 000 time steps (19.4 ps). After the AIMD simulations, configurations of low potential energies were extracted from the trajectories. Those configurations were then subjected to geometry optimization and their zero-point corrected energy was compared with the lowest energy configurations from the DFT calculations mentioned above. All of the AIMD simulations were performed with the Turbomole package.[29]

RESULTS AND DISCUSSION

In a previous theoretical study[7] on Be nanoparticles (nanoclusters and nanocrystals) there were indications of ring-like structures for the fully hydrogenated NPs, Be_nH_{2n}. Herein, we present a detailed study on the structures and energies of small hydrogenated beryllium NPs, for sizes in the range of $n = 3–20$, and examine the prospect of their usage for hydrogen storage, and discuss details of their infrared spectra.

Structures. The ground state structures along with energetically slightly higher stereoisomers are shown in Figure 1. The clusters fall in one of the categories of (a) linear-chain, (b) ring-type, and (c) link-type structures. We systematically use the nomenclature chain to emphasize the linear form of the polymeric type. Most of the structures are moderately to highly symmetric, with only a few energetically low that are nonsymmetric. The linear chain structures are of particular importance since they provide a standard by which comparisons can be made on certain aspects of the other types that lead to strain induced lowing of their energies. The linear chain structures consist of a linear sequence of beryllium atoms that are linked to each other by two hydrogen atoms forming a $-[Be(\mu^2\text{-}H)_2]_n-$ bridge configuration. We can define the direction of two linking H atoms as a vector from one to the other. Successive linking H atoms have alternating directions perpendicular to the chain axis and to each other, as shown in Figure 1. At each end of the linear chain one H atom is located along the chain axis after the terminating Be atoms. The ring structures can be considered as chain structures looped in a ring in such a manner that the two H atoms, originally at the two ends of the chain, are brought together to form a linking pair. As in the case of the chain structures, the directions of successive linking H pairs are alternating, however, in this case they are not perpendicular to each other. The divergence from perpendicular orientations depends on the curvature of the structure, or equivalently on cluster size. The link-type structures are similar to the ring-type but contain at least one cape configuration of three Be atoms and four H atoms that is directly linked to the rest of the structure in the usual manner as described above. This structural type is of increased importance for clusters of odd size.

The symmetry of the structures is noted in Figure 1. All of the chain structures are of high symmetry, specifically D_{2h} for chain structures with an even value n, and D_{2d} for odd values of n in which case a beryllium atom is located at the center of inversion of the chains. For even values of n the ring-type structures also exhibit high symmetry, of $D_{(n/2)d}$. As we shall see, these are the ground state structures for cluster sizes with even values of $n > 8$. For odd values of $n > 9$ the ground state structures are link-type with one cape configuration and all have C_s symmetry. Other structures will be examined in the course of the discussion.

The energy difference between the chain structures and the energetically lowest closed form (ring or link) structures for Be_nH_{2n} NPs is shown in Figure 2. Positive values indicate that the chain structure has lower energy, while negative values indicate that the ring/link structure has lower energy. We find that for n smaller than 10 the chain structures are energetically favorable. For values of n equal or greater than 10, the ground

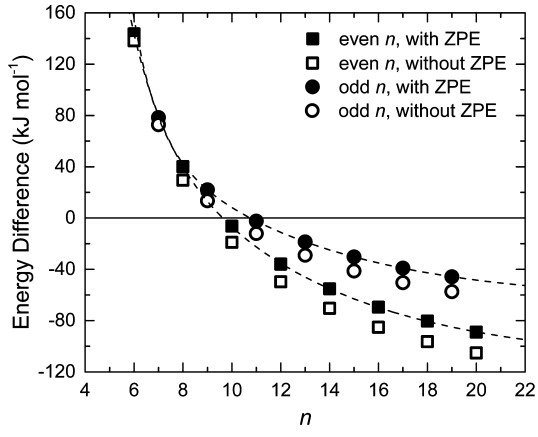

Figure 2. Energy difference between chain and ring-type (for even n) or link-type (for odd n) structures with respect to even (square) and odd (circles) values of n, with (solid) and without (hollow) ZPE contribution.

DOI: 10.1021/jacs.6b00135
J. Am. Chem. Soc. 2016, 138, 3218–3227

state structures are closed form, either ring or link-type. For n = 10 and n = 11 their energy difference compared to the corresponding chain structures is marginal. However, throughout the size ranges examined here this energy difference increases (absolutely) with cluster size indicating that the ring and link structures become more favorable as the nanoparticle size increase. We note that zero point energy corrections only affect slightly the energy differences, by about 7−15 kJ mol^{-1}, which is not enough to alter the outcome of the energy ordering of the structures.

Although in general the energy difference of the chain structures with the energetically lowest closed loop structures increases with size, two distinct trends are observed, that can be seen in Figure 2. For NPs with sizes $n \geq 10$, ring structures with even values of n have lower energies compared to their immediate neighbors in size lowest energy structures. This suggests that ring clusters of even n may be magic.

Binding Energy. To examine this we have calculated the binding energies per beryllium atom, $E_b(Be_nH_m)$, of the closed form structures which we show in Figure 3 for the full range of

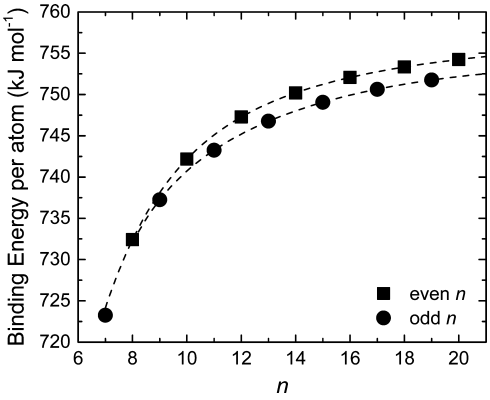

Figure 3. Binding energy per beryllium atom of ring-type and link-type Be_nH_{2n} nanoparticles versus size n. Dashed lines are guides to the eye.

clusters sizes under study. The binding energy per atom is defined as usual by the relation:

$$E_b(Be_nH_m) = [nE(Be) + mE(H) - E(Be_nH_m)]/n \quad (1)$$

where E(H) and E(Be) are the atomic energies of H and Be, and $E(Be_nH_m)$ the total energy of the ring nanoparticles, including the zero-point energy (ZPE). In Figure 3 it can be seen that the even sized ring clusters follow a trend with a slightly increased binding energy per atom compared to the clusters of odd sizes. This energy difference originates from the constraints introduced in the odd sized clusters from the cape configuration that defines the link-type structure. This cape configuration, already mentioned earlier, consists of three beryllium atoms and 4 hydrogen atoms, and can be identified in all the odd sized clusters of C_s symmetry. This is a constrained configuration for the hydrogen atoms that link the cape to the rest of the structure. Furthermore, one of the hydrogen atoms does not link two beryllium atoms, which we will show further along is an energetically higher configuration. Although the magnitude of the energetic difference is small, ring clusters with even values of n are indeed magic. As shown in Figure 1, all of the ring clusters with even sizes are highly symmetric. The symmetry of ring clusters with odd values of n is significantly lower, specifically of C_2 symmetry, as a result of purely geometric reasoning; each beryllium atom is connected to its previous one with two hydrogen atoms. Consecutive pairs of linking hydrogens ideally would form perpendicular relative configurations. In rings with an odd number of such pairs the ring cannot close without compromising this alternating sequence. In Figure 1 in addition to the even sized ring clusters we also show the higher energy ring clusters for n = 9 and n = 11. No dynamically stable ring structures of higher odd sizes were found. Link type structures with even more cape configurations exist for both even and odd sizes, such as the C_s structure for n = 11 and the C_{4v} structure for n = 12, but these are energetically higher mainly due to the additional hydrogen atoms that are introduced in a non linking configuration. Having established the trend, we do not present such configurations for structures larger than n = 12.

Link type structures were also examined for even sized clusters. We systematically find that even sized link type structures with one cape configuration are nonsymmetric (C_1) and higher in energy than same sized clusters with two cape configurations. Again, the reason is purely geometric; one cape configuration leaves an odd number of beryllium atoms, or equivalently an even number of linking hydrogen pairs, which cannot close the structure without compromising the alternating sequence of perpendicular hydrogen pair configurations. With two symmetrically placed cape configurations the sequence is achievable, although strains induced by the curvature of the structures still remain.

Curvature Induced Structural Strain. The chain structures are useful to estimate the decrease in energy from strain induced on the structures by curvature or twist. We consider the small Be_3H_6 chain cluster shown in Figure 4, and

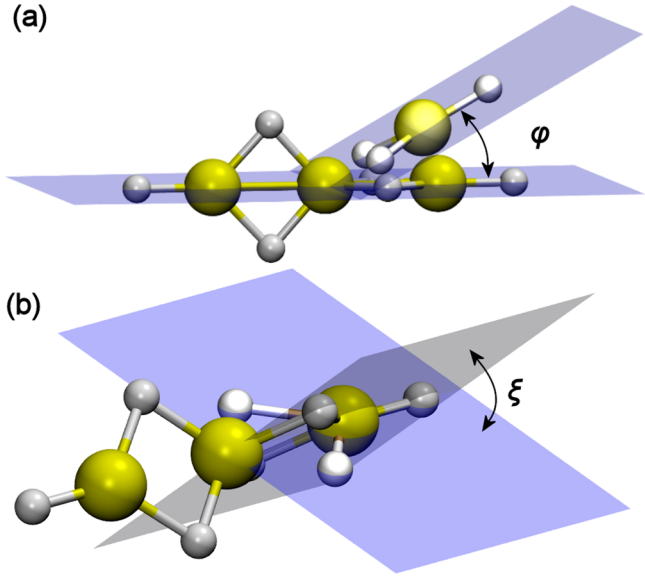

Figure 4. Rotation of the (a) bending angle φ and (b) torsion angle ξ, used for the rigid potential energy surface scan performed on the Be_3H_6 chain cluster. Corresponding energy changes are given in Table 1.

examine the changes in energy through a rigid potential energy surface (PES) scan upon two distinct structural changes: (a) an angle bending by an angle φ between three sequential beryllium atoms while retaining a perpendicular orientation between the directions (as defined above) of intermediate linking hydrogen pairs, and (b) a twist of the dihedral angle by an amount of ξ, between the initially perpendicular directions of the two sequential linking hydrogen pair directions. In each case of the Figures 4 one plane represents the originally undistorted plane,

DOI: 10.1021/jacs.6b00135
J. Am. Chem. Soc. 2016, 138, 3218−3227

and the other one is the new configuration after the angle bend or dihedral angle twist. We chose the smallest structure in order to benchmark the results obtained at the M06/cc-pVTZ level against those using the computationally more demanding high accuracy coupled-cluster theory, including singlet and doublet excitations (CCSD), and CCSD(T) which additionally includes triplet excitations noniteratively,[23,24] also using the cc-pVTZ basis set.[22] The initial geometries prior to the PES scan were optimized at the M06/cc-pVTZ and CCSD/cc-pVTZ levels, respectively. As can be seen in Table 1 the results based on the

Table 1. Changes in Energy, ΔE, with Respect to the Corresponding Relaxed Structure, from the Rigid Potential Energy Surface Scan Performed on the Be_3H_6 Chain Cluster upon Rotation of the Bending Angle φ and Torsion Angle ξ (as Shown in Figure 4)

φ (degrees)	M06 (kJ mol^{-1})	CCSD (kJ mol^{-1})	CCSD(T) (kJ mol^{-1})
0	0.00	0.00	0.00
7.5	1.17	1.15	1.11
15	4.71	4.62	4.49
22.5	10.70	10.52	10.22
30	19.25	18.98	18.41
ξ (degrees)	M06 (kJ mol^{-1})	CCSD (kJ mol^{-1})	CCSD(T) (kJ mol^{-1})
0	0.00	0.00	0.00
7.5	1.71	1.70	1.70
15	6.79	6.78	6.76
22.5	15.14	15.13	15.08
30	26.58	26.56	26.48

M06 functional are in very good agreement with the coupled-cluster values, with relative errors in the range of 4.6%−5.1% for the angles φ, and at 0.4%−0.5% for the dihedral angles ξ. It is also clear that the strain energy has a nonlinear dependence on the angles φ and ξ. For smaller ring structures that have higher curvature, this results in larger increases in energies with respect to the unstrained chain structures. Only when sizes of $n = 10$ are reached the strain from these angular distortions becomes low enough for the closed form structures to become energetically favorable. We note that in the angular PES scan by constraining the direction of sequential linking hydrogen atoms to perpendicular orientations the resulting energy changes are an *upper* limit, since relaxation of the torsion orientations would decrease the change in energy. Effectively, there are two competing mechanisms that determine the energetic outcome; the increase in energy from the curvature induced strain, and the lowering in energy that corresponds to the energy difference between two terminating hydrogen atoms configurations (that we denote as Y, residing on the chain axis) and two hydrogen atoms in a (energetically more favorable) linking configuration (that we denote as X).

Be−H Bond Energies. The chain structures also offer us the means to calculate the theoretical maximum limit of the energy benefit on going from a chain structure, which has two hydrogen atoms in a Y configuration, to a ring structure, in which the same two hydrogen atoms would have an X configuration. We denote as E_Y the Be−H bond energy in a Y configuration, and as E_X the Be−H bond energy in an X configuration, and effectively partition the binding of the chain structures to linking Be−H bonds. In a chain there are two Y configurations that correspond overall to $2E_Y$ energies. In a ring structure two hydrogen atoms form four X type Be−H bonds that correspond overall to $4E_X$. Since only even sized structures systematically form ring structures, we examine the energy difference between structures with sequential even values of n. With some algebra it can readily be found that

$$4E_X = 1/2[E_B(Be_{n+2}H_{2(n+2)}) - E_B(Be_nH_{2n})]$$

and

$$2E_Y = 1/2[(n+1)E_B(Be_nH_{2n}) - (n-1)E_B(Be_{n+2}H_{2(n+2)})]$$

where $E_B(Be_nH_{2n})$ and $E_B(Be_{n+2}H_{2(n+2)})$ are the binding energies, $E_B = nE_b$, of the Be_nH_{2n} and $Be_{(n+2)}H_{2(n+2)}$ chain clusters, respectively. Thus, the total energy gain simply from changing two Y configurations into X configurations is

$$\Delta E_{2Y\rightarrow 4X} = \frac{n}{2}E_B(Be_{n+2}H_{2(n+2)}) - \frac{n+2}{2}E_B(Be_nH_{2n}) \quad (2)$$

The limit value of this quantity as n goes to infinity is an upper bound of the energy benefit that can be obtained upon closing a chain structure into a ring structure, in a similar manner as imposing periodic boundary conditions (PBC) on the two ends of the chains. We note that this quantity does not account for the curvature upon such a change. In Figure 5 we have plotted

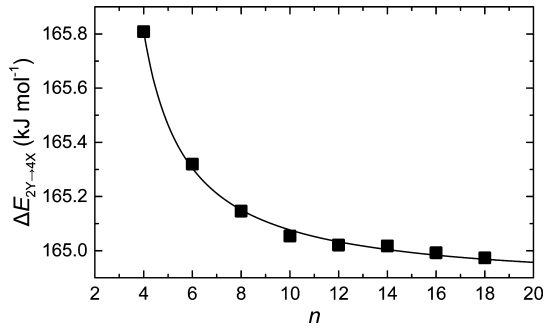

Figure 5. Energy gain from changing 2 Y-type to 4 X-type Be−H bonds as a function of cluster size. The line is an exponential decay fit with an asymptotic value of 164.86(2) kJ mol^{-1}.

the energy gain, $\Delta E_{2Y\rightarrow 4X}$, from changing 2 Y-type to 4 X-type Be−H bonds as a function of cluster size. The energy converges very fast to the asymptotic value of 164.86(2) kJ mol^{-1}. As expected, this limit value is larger than the energy differences shown in Figure 2. The corresponding asymptotic values for the Y-type and X-type Be−H bond energies are E_Y = 296.55 kJ mol^{-1} and E_X = 189.51 kJ mol^{-1}, respectively. The experimental dissociation energy of BeH in gas phase at 298 K is reported at 226 kJ mol^{-1}, and 222 kJ mol^{-1} at 0 K,[30] which falls between the E_Y and E_X values calculated herein, and is in excellent agreement with the corresponding value, E_B(BeH) = 219.7 kJ mol^{-1}, that we have calculated using the M06 functional.

Polymerization Energy. In addition to the binding energy we also calculated the polymerization energy with respect to the BeH_2 monomers, defined as

$$E_{pol}(Be_nH_m) = E(BeH_2) - E(Be_nH_{2n})/n \quad (3)$$

In Figure 6 we show the dependence of the polymerization energy on the size of the chain NPs. The lines are exponential fits to the energy values with and without ZPE corrections, with asymptotic values of 140.413(3) kJ mol^{-1} (1.455 eV) and 158.225(3) kJ mol^{-1} (1.640 eV), respectively (details of the fits

DOI: 10.1021/jacs.6b00135
J. Am. Chem. Soc. 2016, 138, 3218−3227

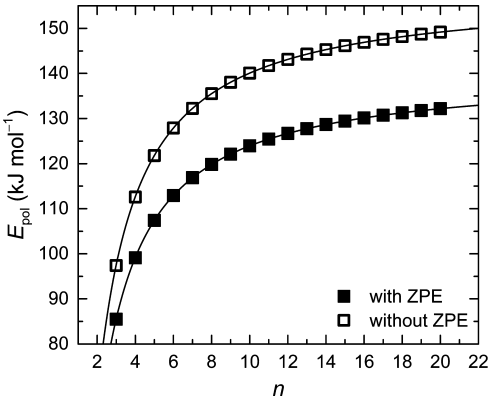

Figure 6. Polymerization energy per BeH_2 monomer as a function of chain size. The lines are exponential growth fits to the data points, with asymptotic values of 140.413(3) kJ mol^{-1} and 158.225(3) kJ mol^{-1} with and without ZPE corrections, respectively.

are given in the Supporting Information). In their work Abdurahman et al.[12] have performed high accuracy CCSD and CCSD(T) calculations on the infinite polymeric structures, with the unit cells optimized at the respective level of theory. Their reported polymerization energies (per monomer) are 1.70 and 1.74 eV at the CCSD and CCSD(T) level, respectively. The agreement of these values, that do not include ZPE corrections, with our corresponding non-ZPE corrected asymptotic values are exceptional, especially if one considers the difference in level of theories (DFT vs wave function theory) and methodologies (periodic vs real space calculations). This result further validates the suitability of our choice to use the M06 functional. Our approach has the added advantage that it permits for the calculation of the energies for each cluster size. From the ZPE corrected polymerization energies of the individual chain clusters shown in Figure 6 we find that these corrections have a significant impact and need to be considered. Other values given in the literature (none of which include ZPE corrections) for the polymerization energy are by Wang et al. for sizes of n = 2−8 at 1.43 eV (33 kcal mol^{-1}),[10] and by Mire et al. for the Be_2H_4 dimer at 1.41−1.47 eV (32.6−33.8 kcal mol^{-1}).[31] When cluster sizes are taken into account the aforementioned reported values significantly overestimate the corresponding polymerization energy. We provide our results (with and without ZPE corrections) as accurate reference values tabulated in the Supporting Information.

Hydrogen Desorption. From the calculations and the structural details of the chain structures, as well as previous results,[7] there is an indication that the chain structures can retain additional H_2 molecules. For example, in Figure 7 we show optimized structures for Be_6H_{12}, Be_6H_{14} and Be_6H_{16}. Adding two H atoms to Be_6H_{12} results in the formation of an H_2 molecule in close proximity to the Be atom at one end of the chain type NP. We opted to examine the dynamic stability of such configurations since they could possibly offer an alternative and complementary mechanism to capture hydrogen. The importance lies in the prospect made evident for example in the smallest chains, with n = 2, in which case the hydrogen weight percentage (wt %) can reach up to 30.8 wt %. This value of course reduces as the particle sizes increase. Table 2 shows the hydrogen weight percentage (wt %) of Be_nH_{2n+4} clusters. Taking into account all H atoms, the wt % starts from 22.9% for n = 6 and reaches 30.8% for n = 2 which is seemingly one of the highest, if not the highest, percentage rates. On the other hand,

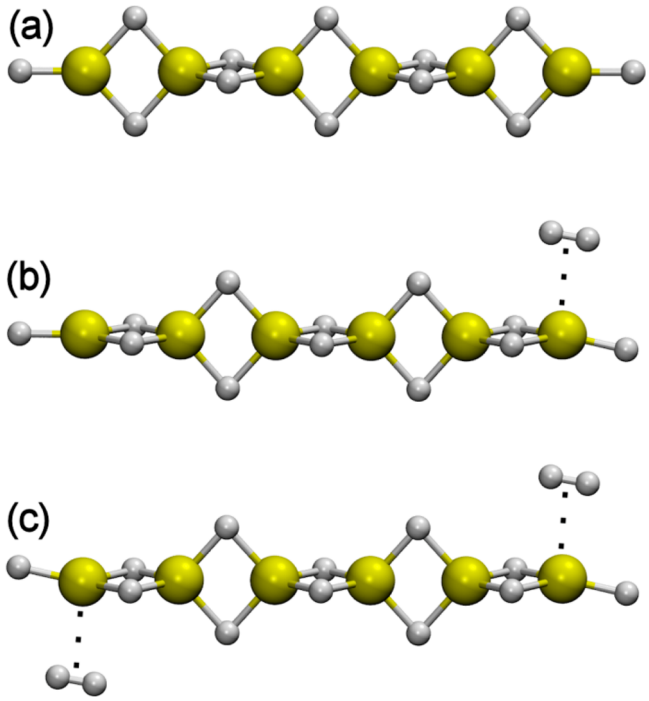

Figure 7. Chain structures for (a) Be_6H_{12}, (b) Be_6H_{14}, and (c) Be_6H_{16}.

Table 2. Hydrogen Weight Percentage for Be_nH_{2n+4} Clusters

n	wt % (all H)	wt % (only $2H_2$)
2	30.8	15.4
3	27.0	10.8
4	25.0	8.3
5	23.7	6.8
6	22.9	5.7

assuming that only the additional two H_2 molecules contribute to the hydrogen storage while the rest of the H atoms remain bonded to the cluster, the hydrogen wt % starts at 5.7% for n = 6 and reaches the value of 15.4% for n = 2 which is still one the highest percentage rates.

First we calculate the normalized per H_2 mole desorption energy of the saturated chain structures (stoichiometric NPs). In the general case of a nonstoichiometric Be_nH_m nanocluster the normalized per H_2 mole desorption energy, $\Delta E_d(Be_nH_m)$, is calculated using the relation:

$$\Delta E_d(Be_nH_m) = E(H_2) + 2[E(Be_n) - E(Be_nH_m)]/m \quad (4)$$

where $E(H_2)$, $E(Be_n)$, and $E(Be_nH_m)$ are the total energies of the H_2 molecule, and the Be_n, Be_nH_m clusters, respectively.

In Figure 8a we show the normalized per H_2 mole desorption energy of small sized (saturated) stoichiometric chain nanoparticles. We emphasize that these values are with respect to structures fully optimized at the M06/cc-pVTZ level and include ZPE corrections to the total energies in eq 4. These results are in good agreement with the corresponding values given in our previous work,[7] which further testifies to the suitability of our therein chosen strategy to obtain the structures of the nanoparticles that reached large sizes. However, the desorption energies are extremely high, in the range of 140−240 kJ mol^{-1} for the small sized Be_nH_{2n} chain clusters rendering them impractical for any real hydrogen storage application.

Calculation of the corresponding desorption energies for the oversaturated chain structures proved to be more demanding.

DOI: 10.1021/jacs.6b00135
J. Am. Chem. Soc. 2016, 138, 3218−3227

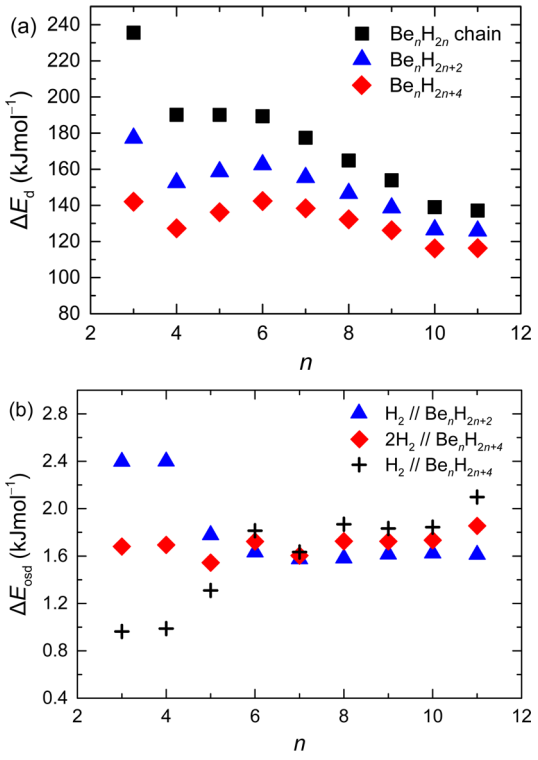

Figure 8. (a) Normalized per H_2 mole desorption energy of the $Be_nH_{2(n+k)}$ chain clusters, ΔE_d (see text, eq 4), versus the number of Be atoms (n) for $k = 0$ (black squares), $k = 1$ (blue triangles), and $k = 2$ (red rhombi). (b) Normalized per oversaturated H_2 mole desorption energy of the $Be_nH_{2(n+k)}$ chain clusters, ΔE_{osd} (see text, eq 5), versus the number of Be atoms, n, for desorption of 1 H_2 from $Be_nH_{2(n+1)}$ (blue triangles), 2 H_2 from $Be_nH_{2(n+2)}$ (red rhombi), and 1 H_2 from $Be_nH_{2(n+2)}$ (black crosses). Energy values include ZPE corrections.

Upon addition of two hydrogen atoms and subsequent structural optimization, without symmetry constraints, an H_2 molecule is formed in the vicinity of a terminating Be atom. However, for many of these structures an imaginary frequency was found in spite of the tight convergence criteria that were imposed. The imaginary mode is the libration of the H_2 molecule with a preferred orientation approximately along the axis of the chain structure. The procedure usually followed of slightly distorting the structure along the eigenvector of the imaginary mode and subsequent structural reoptimization proved inadequate to remove the imaginary mode. Imposing even more strict convergence criteria as well as increasing the size of the basis set also proved inadequate to remove these modes. At this point we opted to examine the effect of the density of the integration grids on the energies and frequencies of the vibrational modes examining the Be_7H_{16} oversaturated chain cluster as a test case, that we present in the Supporting Information. On the basis of these results, to calculate the desorption energies of the oversaturated chains we have chosen the very dense (150,974) grid for integration combined with the (75,302) CPKS grid.[32−34]

As shown in Figure 8a, compared to the case of the stoichiometric chain clusters, the desorption energy range lowers significantly for the corresponding oversaturated clusters with an adhered H_2 molecule (see Figure 7), and reaches 125−180 kJ mol^{-1}, and at 115−140 kJ mol^{-1} for two adhered H_2 molecules. This lowering in energy is misleading in that for the oversaturated clusters the as calculated desorption energy in effect averages between two distinct types of hydrogen desorption mechanisms; that of the linking hydrogen atoms of the chain structure at high energy values, and another of the physisorbed H_2 molecule at low energies. For this reason we define an alternative normalized per H_2 mole desorption energy, ΔE_{osd}, which quantifies the energy required for a partial desorption of a total of k H_2 molecules from the oversaturated $Be_nH_{2(n+k)}$ cluster,

$$E_{osd}(Be_nH_{2(n+k)}) = E(H_2) + [E(Be_nH_{2n}) - E(Be_nH_{2(n+k)})]/k \quad (5)$$

where $E(H_2)$, $E(Be_nH_{2n})$, and $E(Be_nH_{2(n+k)})$ are the total energies of the H_2 molecule, and the Be_nH_{2n}, and $Be_nH_{2(n+k)}$ clusters, respectively. The corresponding results are shown in Figure 8b.

Three separate cases are shown that correspond to desorption of (a) a single H_2 molecule from the $Be_nH_{2(n+1)}$ chain cluster (shown with blue triangles), (b) two H_2 molecules from the $Be_nH_{2(n+2)}$ chain cluster (shown with red rhombi), and (c) one H_2 molecule from the $Be_nH_{2(n+2)}$ chain cluster (shown with black crosses) that leaves back the still oversaturated $Be_nH_{2(n+1)}$ chain cluster. We have included the $n = 11$ case only for completeness and since the energy difference from the ground state (ring) cluster is very small. Edge effects seem only to play a role for very small cluster sizes of $n < 6$. In these small sized clusters with 2 adsorbed H_2 molecules the energy required to remove 1 H_2 molecule is notably less than that required when only a single H_2 molecule is adsorbed. For larger sizes all three cases give approximately the same E_{osd}, which is expected when processes that take place on one end of the chain do not affect the other end (and keeping in mind that E_{osd} is a normalized per H_2 quantity). In these cases E_{osd} is in the range 1.6−1.8 kJ mol^{-1}. Nevertheless, in both of these cases the desorption energy of the oversaturated chains remains very low for any practical application. This finding is further corroborated by the experimental work of Ray et al., who used high-resolution electron energy loss spectroscopy and thermal desorption spectroscopy, and reported the lack of any evidence of H_2 molecular adsorption on Be (0001) surface at the temperatures that they investigated which were higher than 90 K.[35]

To examine the effect of zero-point energies on E_{osd}, we repeated the calculations without including ZPE corrections, the results of which are shown in Figure S1 of the Supporting Information. It is easily seen that both the range of values, as well as the size dependence, change significantly. The so calculated energy range increases significantly and is between 11.5−12.0 kJ mol^{-1} and decays with size. It is obvious that without ZPE corrections one might be mislead to conclude that this type of adsorption (molecular hydrogen on small chain type NPs) holds promise for hydrogen storage applications (with optimum values ∼15−25 kJ mol^{-1}[36−40]).

Ab Initio Molecular Dynamics. A method that turned out very efficient in scanning the potential energy hypersurface of the NPs was by performing AIMD simulations at high temperatures. This resulted in, or reproduced, some of the lowest energy Be_nH_{2n} nanoclusters. Figure 9 illustrates configurations of Be_4H_8, Be_8H_{16} and $Be_{14}H_{28}$ nanoparticles at initial and advanced stages the AIMD simulations, that were performed at $T = 700$, 1300, and 1250 K, respectively. In Figure 10 we show the potential energy (PE) of those three nanoparticles with respect to simulation time. The PE curve

DOI: 10.1021/jacs.6b00135
J. Am. Chem. Soc. 2016, 138, 3218−3227

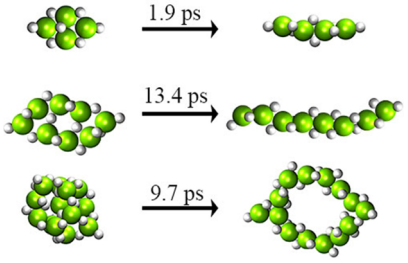

Figure 9. Configurations of Be_4H_8, Be_8H_{16} and $Be_{14}H_{28}$, clusters before (left) and after (right) the AIMD simulations. The numbers above the arrows display the time span between the initial and the final configurations of the nanoparticles.

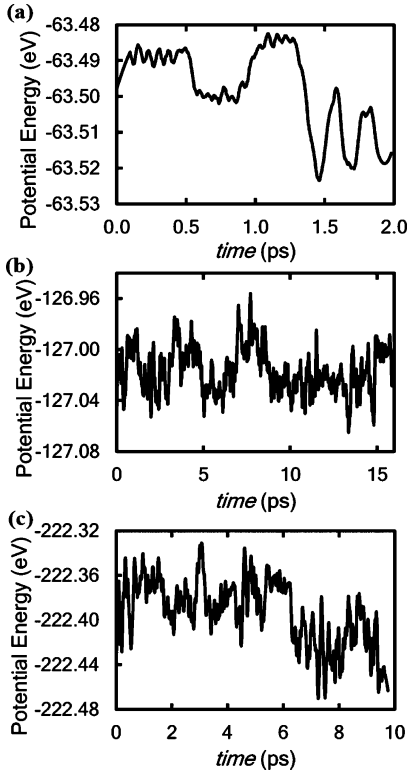

Figure 10. Potential energy with respect to AIMD simulation time for (a) Be_4H_8, (b) Be_8H_{16} and (c) $Be_{14}H_{28}$. For clarity, the diagrams were smoothed with a Savitzky–Golay filter.[41]

in Figure 10a that refers to Be_4H_8 cluster features a steep descent at ~1.3 ps indicating a structural transition that leads to a lower energy conformation. The corresponding curve for Be_8H_{16}, with an initial low-energy rhombus-like shape conformation, displays a more complicated behavior. Nevertheless, after ~13 ps it finally transformed to a linear chain.

Note that this is imprinted in the PE plot of Figure 10b, which features a steep minima at ~13 ps. Remarkably, even the $Be_{14}H_{28}$ nanoparticle which was initialized at a very high energy configuration, after ~6.2 ps displayed a transition to a lower energy configuration (featuring a steep descent in the PE in Figure 10c), leading to a link type structure as shown in Figure 9.

IR Spectra. In order to facilitate the experimental characterization of the theoretically obtained structures, we have calculated infrared (IR) spectra for all of the ground state and energetically low isomers of Figure 1. To better compare the calculated with the experimentally measured frequencies reported by Wang et al.[10] we have additionally computed the IR spectrum of H–Be(μ^2-H)$_2$Be–H and provide the calculated and measured results, along with the corresponding scaling factors, of modes with strong absorption in Table 3.

Table 3. Vibrational Mode Frequencies of HBe(μ^2-H)$_2$BeH[a]

vibrational mode	sym	calculated	measured[b]	scale factor
Be–H stretch	b_{1u}	2161	2065	0.956
Be–H–Be stretch	b_{2u}	1621	1577	0.973
Be–H–Be stretch	b_{1u}	1457	1423	0.977
Be–H–Be out-of-plane	b_{3u}	940	923	0.982
Be–H–Be in-plane	b_{2u}	589	585	0.993

[a]Comparison between theoretically calculated values using M06/cc-pVTZ, experimentally measured within a solid neon matrix, and the resulting scaling factors. Values are given in cm^{-1}. [b]Values taken from ref 10.

In Figure 11a we show the IR absorbance in the, 1300–1500 cm^{-1} region, of the chain structures for all sizes (up to n = 20).

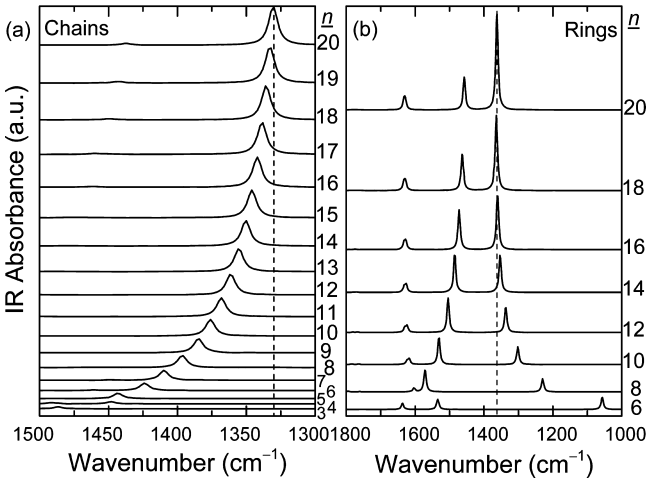

Figure 11. Infrared spectra for the 1300–1500 and 1000–1800 cm^{-1} regions of Be_nH_{2n} (a) chain and (b) ring type structures. Cluster sizes, n, are given alongside of the plots. The corresponding full spectra are given in the Supporting Information.

We collectively provide the full IR spectra for all of the structures of Figure 1 in the Supporting Information. The chain clusters exhibit several noteworthy infrared absorption peaks with one prominent and five moderate peaks. In contrast to the low intensity peaks, the frequency of the strongest peak exhibits a size dependence, specifically, the frequency decreases with size, as shown in Figure 11a. This b_2 symmetry mode is a coherent oscillation along the growth direction of the chain of all the linking hydrogen atoms. This frequency, that decrease in steps of ~12–8 cm^{-1}, provides an explanation for the very similar experimentally observed stepwise peaks in the 1330–1410 cm^{-1} region (using the appropriate scaling factor of 0.975), if they are attributed to chain structures of sizes up to n = 12. The next most prominent peak, centered ~1633 cm^{-1}, can be considered as complementary to the primary one. It consists of two doubly degenerate modes (i.e., each of e symmetry), with frequencies at 1631 and 1635 cm^{-1}, respectively, independent of cluster size, that correspond to vibrations of linking hydrogen atoms in a direction perpendicular to the chain axis, i.e., each pair along their respective pair directions as defined earlier in the

DOI: 10.1021/jacs.6b00135
J. Am. Chem. Soc. 2016, 138, 3218–3227

discussion of the structures. A very characteristic mode of the chain structures, but of lower intensity, is the b_2 symmetry mode at 2163 cm^{-1} which corresponds to antisymmetric Be−H bond stretching of the terminal hydrogen atom. Also very characteristic, but of significantly lower intensities, are two doubly degenerate modes (each of e symmetry) at 485 and 580 cm^{-1} that correspond to angle bending vibrations of the terminal hydrogen atoms.

In their work, Wang et al. measured the infrared spectrum of Be_nH_{2n} particles within a solid neon (and hydrogen) matrix and attributed them to a chain structure, with a presumed maximum size of $n = 8$. Although spectral features such as the existence of the observed high frequency modes can be uniquely attributed to chain clusters (namely, stretching modes of the terminal hydrogen atoms), other modes such as those observed after ultraviolet irradiation (with $\lambda = 220$ nm) at 1495 cm^{-1}, 1541 cm^{-1}, 1558 and 1582 cm^{-1}, cannot. However, modes are found in that region (scaling factor 0.975) of the computed spectra of ring type clusters with a size of $n = 8$ and $n = 10$, that we show in Figure 11b, and may offer an explanation for the observed peaks. For the $n = 10$ ring cluster these modes correspond to a doubly degenerate e_{1u} mode at 1531 cm^{-1} of in-plane coherent tangent vibrations of the inner hydrogen atoms, and at higher frequencies, a doubly degenerate e_{1u} symmetric mode at 1617 cm^{-1} of hydrogen linking pairs oscillating along their direction coherently with neighboring pairs (resembling an acoustic mode), and a similar nearby a_{2u} symmetry mode at 1624 cm^{-1} (in this case resembling an optical mode).

The link type structures exhibit much richer IR spectra (shown in Figure 12). A common feature of all the link type

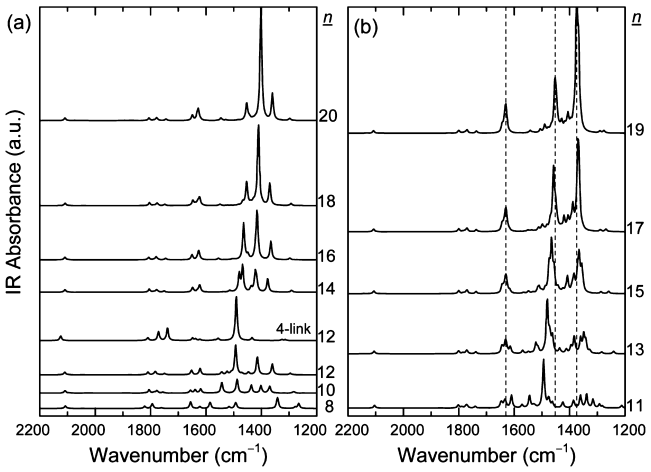

Figure 12. Infrared spectra for the 1200−2200 cm^{-1} regions of link type Be_nH_{2n} clusters of (a) even and (b) odd sizes. Cluster sizes, n, are given alongside of the plots. The corresponding full spectra are given in the Supporting Information.

structures is the high frequency peak at 2104 cm^{-1} which corresponds to the stretching mode of the lone (nonbridging) hydrogen atom of the cape configuration. Although the frequency of this mode is near to that of the terminal hydrogen stretching mode of the chain structures, it is not high enough to be attributed to the high energy mode observed by Wang et al., who do not report any other nearby peaks. Also, this mode is not size dependent (or only very mildly dependent for small cluster sizes) and does not depend on the number of cape configurations present in the clusters. Another common feature among the link type clusters are three peaks of moderate intensity just below 1800 cm^{-1}. These peaks consist of several modes, with the three dominant ones, at 1741 cm^{-1} (a″ symmetry), 1772 cm^{-1} (a′ symmetry), and 1802 cm^{-1} (a′ symmetry), being either antisymmetric or symmetric vibrations mainly of the remaining hydrogen atoms of the cape configurations. For the odd sized link type clusters a very characteristic mode with a small frequency size dependence is located at 1339 cm^{-1} for $n = 11$ and at 1374 cm^{-1} for $n = 19$ (intermediate sizes have intermediate frequencies) results from in-plane coherent vibrations mainly of the outer hydrogen atoms and exhibits a strong intensity size dependence (increases with size). The corresponding mode of the inner hydrogen atoms is located at 1494 cm^{-1} for $n = 11$ and at 1453 cm^{-1} for $n = 19$, and with the same intensities. The even sized link type clusters also exhibit similar modes, which for the inner (outer) hydrogen atoms are located at 1504 (1337) cm^{-1} for $n = 12$, and at 1457 (1362) cm^{-1} for $n = 20$. Also, the peak centered ∼1630 cm^{-1} consists of a doubly degenerate mode at 1629 cm^{-1} for $n = 20$, and an analogous antisymmetric mode of b_2 symmetry at 1633 cm^{-1}, of the hydrogen linking pairs along their respective directions.

CONCLUSIONS

Ground state structures and energetically low lying structures of Be_nH_{2n} nanoparticles have been predicted and presented, for $3 \leq n \leq 20$. The computations were performed within the framework of DFT using the meta-hybrid M06 functional and the cc-pVTZ basis set, the results from which were found in very good agreement when compared against those from high accuracy CCSD(T). We have shown that the ground state structures of clusters with sizes for n up to 9 are linear (polymeric) form. For larger sizes the type of the ground state structures are ring type or link type for even and odd values of n, respectively. For $n = 10$ and 11 the energy difference between polymeric and ring/link type structures is marginal. Almost all of the structures are moderately to highly symmetric. We provide the size dependence of the binding energy of the structures and find that ring type structures (i.e., with even sizes, n) are magic. The polymerization energy of the polymer forms has an asymptotic value of 140.413(3) kJ mol^{-1} when ZPE corrections are applied. When ZPE corrections are not included this value reaches 158.225(3) kJ mol^{-1} (that agrees with high level noncorrected values from the literature). We distinguish between Y-type and X-type Be−H bonds and compute their energies that have asymptotic values of $E_Y = 296.55$ kJ mol^{-1} and $E_X = 189.51$ kJ mol^{-1}, respectively. We presume on the accuracy of these values based on the agreement of our calculated BeH dissociation energy of 219.7 kJ mol^{-1} that is very near the experimental one of 222 kJ mol^{-1} (for 0 K). We have assessed the possibility of using small chain type clusters for applications in hydrogen storage and find them *unsuitable* for this purpose. This conclusion is drawn based on the low values of desorption energies of molecular hydrogen for the oversaturated species, that *include* (well converged) ZPE corrections. When such corrections are not included the energy values are higher and may easily lead to erroneous conclusions. We show that a procedure that can lead to energetically low lying structural configurations is by employing AIMD simulations at high temperatures and for moderate simulation times. The procedure assisted our search for low energy structural configurations. This approach proved effective even in cases which energetically high initial structures were used. Finally, we provide infrared spectra

DOI: 10.1021/jacs.6b00135
J. Am. Chem. Soc. 2016, 138, 3218−3227

for all the structures under study along with an extensive discussion on the vibrational modes of characteristic and high absorbance peaks, and compare to experimental results when available.

■ ASSOCIATED CONTENT

Supporting Information

The Supporting Information is available free of charge on the ACS Publications website at DOI: 10.1021/jacs.6b00135.

Polymerization energy, X and Y type Be−H bond energies, zero point energy corrections, integration and CPKS grids, infrared spectra, coordinates of structures. (PDF)

■ AUTHOR INFORMATION

Corresponding Author

*koukaras@physics.upatras.gr

Notes

The authors declare no competing financial interest.

■ ACKNOWLEDGMENTS

A. S. acknowledges support through the project "Multiscale Simulations of Complex Polymer Systems" (MuSiComPS) by the Limmat Foundation, Zurich, Switzerland.

■ REFERENCES

(1) Maximilian, F. *Nanotechnology* **2009**, *20* (20), 204009.
(2) Bérubé, V.; Radtke, G.; Dresselhaus, M.; Chen, G. *Int. J. Energy Res.* **2007**, *31* (6−7), 637−663.
(3) Koukaras, E. N.; Zdetsis, A. D.; Sigalas, M. M. *J. Am. Chem. Soc.* **2012**, *134* (38), 15914−15922.
(4) Barbagiovanni, E. G.; Lockwood, D. J.; Simpson, P. J.; Goncharova, L. V. *Appl. Phys. Rev.* **2014**, *1* (1), 011302.
(5) Kelly, M. Perspective on the Storage of Hydrogen: Past and Future. In *Fuel Cells and Hydrogen Storage*; Bocarsly, A., Mingos, D. M. P., Eds.; Springer: Berlin, 2011; Vol. *141*, pp 169−201.
(6) Wu, H. *ChemPhysChem* **2008**, *9* (15), 2157−2162.
(7) Zdetsis, A. D.; Sigalas, M. M.; Koukaras, E. N. *Phys. Chem. Chem. Phys.* **2014**, *16* (27), 14172−14182.
(8) Allouche, A.; Oberkofler, M.; Reinelt, M.; Linsmeier, C. *J. Phys. Chem. C* **2010**, *114* (8), 3588−3598.
(9) Ganchenkova, M. G.; Borodin, V. A.; Nieminen, R. M. *Phys. Rev. B: Condens. Matter Mater. Phys.* **2009**, *79* (13), 134101.
(10) Wang, X. F.; Andrews, L. *Inorg. Chem.* **2005**, *44* (3), 610−614.
(11) Lingam, C. B.; Babu, K. R.; Tewari, S. P.; Vaitheeswaran, G. *Comput. Theor. Chem.* **2011**, *963* (2−3), 371−377.
(12) Abdurahman, A.; Shukla, A.; Dolg, M. *J. Chem. Phys.* **2000**, *112* (10), 4801−4805.
(13) Smith, G. S.; Johnson, Q. C.; Smith, D. K.; Cox, D. E.; Snyder, R. L.; Zhou, R. S.; Zalkin, A. *Solid State Commun.* **1988**, *67* (5), 491−494.
(14) Mo, O.; Yanez, M.; Alkorta, I.; Elguero, J. *J. Chem. Theory Comput.* **2012**, *8* (7), 2293−2300.
(15) Virot, F.; Barrachin, M.; Vola, D. *Fusion Eng. Des.* **2015**, *98*−*99*, 2219−2222.
(16) Virot, F.; Barrachin, M.; Souvi, S.; Cantrel, L. *Fusion Eng. Des.* **2014**, *89* (7−8), 1544−1550.
(17) Hirai, T.; Maier, H.; Rubel, M.; Mertens, P.; Neu, R.; Gauthier, E.; Likonen, J.; Lungu, C.; Maddaluno, G.; Matthews, G. F.; Mitteau, R.; Neubauer, O.; Piazza, G.; Philipps, V.; Riccardi, B.; Ruset, C.; Uytdenhouwen, I. *Fusion Eng. Des.* **2007**, *82* (15−24), 1839−1845.
(18) Bernath, P. F.; Shayesteh, A.; Tereszchuk, K.; Colin, R. *Science* **2002**, *297* (5585), 1323−1324.
(19) Perdew, J. P.; Burke, K.; Ernzerhof, M. *Phys. Rev. Lett.* **1996**, *77* (18), 3865−3868.
(20) Schäfer, A.; Huber, C.; Ahlrichs, R. *J. Chem. Phys.* **1994**, *100* (8), 5829−5835.
(21) Zhao, Y.; Truhlar, D. *Theor. Chem. Acc.* **2008**, *120* (1−3), 215−241.
(22) Dunning, T. H. *J. Chem. Phys.* **1989**, *90* (2), 1007−1023.
(23) Pople, J. A.; Head-Gordon, M.; Raghavachari, K. *J. Chem. Phys.* **1987**, *87* (10), 5968−5975.
(24) Raghavachari, K.; Trucks, G. W.; Pople, J. A.; Head-Gordon, M. *Chem. Phys. Lett.* **1989**, *157* (6), 479−483.
(25) Frisch, M. J.; Trucks, G. W.; Schlegel, H. B.; Scuseria, G. E.; Robb, M. A.; Cheeseman, J. R.; Scalmani, G.; Barone, V.; Mennucci, B.; Petersson, G. A.; Nakatsuji, H.; Caricato, M.; Li, X.; Hratchian, H. P.; Izmaylov, A. F.; Bloino, J.; Zheng, G.; Sonnenberg, J. L.; Hada, M.; Ehara, M.; Toyota, K.; Fukuda, R.; Hasegawa, J.; Ishida, M.; Nakajima, T.; Honda, Y.; Kitao, O.; Nakai, H.; Vreven, T.; Montgomery Jr., J. A.; Peralta, J. E.; Ogliaro, F.; Bearpark, M. J.; Heyd, J.; Brothers, E. N.; Kudin, K. N.; Staroverov, V. N.; Kobayashi, R.; Normand, J.; Raghavachari, K.; Rendell, A. P.; Burant, J. C.; Iyengar, S. S.; Tomasi, J.; Cossi, M.; Rega, N.; Millam, N. J.; Klene, M.; Knox, J. E.; Cross, J. B.; Bakken, V.; Adamo, C.; Jaramillo, J.; Gomperts, R.; Stratmann, R. E.; Yazyev, O.; Austin, A. J.; Cammi, R.; Pomelli, C.; Ochterski, J. W.; Martin, R. L.; Morokuma, K.; Zakrzewski, V. G.; Voth, G. A.; Salvador, P.; Dannenberg, J. J.; Dapprich, S.; Daniels, A. D.; Farkas, Ö.; Foresman, J. B.; Ortiz, J. V.; Cioslowski, J.; Fox, D. J. *Gaussian 09*, C.01; Gaussian, Inc.: Wallingford, CT, 2009.
(26) Weigend, F.; Ahlrichs, R. *Phys. Chem. Chem. Phys.* **2005**, *7* (18), 3297−3305.
(27) Nosé, S. *J. Chem. Phys.* **1984**, *81* (1), 511−519.
(28) Hoover, W. G. *Phys. Rev. A: At., Mol., Opt. Phys.* **1985**, *31* (3), 1695−1697.
(29) *TURBOMOLE*; TURBOMOLE GmbH: Karlsruhe, Germany, 1989−2007.
(30) Darwent, B. d. *National Bureau of Standards (U.S.), National Standards Reference Data Series* **1970**, *31*, 52.
(31) Mire, L. W.; Wheeler, S. D.; Wagenseller, E.; Marynick, D. S. *Inorg. Chem.* **1998**, *37* (12), 3099−3106.
(32) Lebedev, V. I. *USSR Computational Mathematics and Mathematical Physics* **1976**, *16* (2), 10−24.
(33) Lebedev, V. I.; Skorokhodov, A. L. *Russ. Acad. Sci., Dokl., Math.* **1992**, *45* (3), 587−592.
(34) Gill, P. M. W.; Johnson, B. G.; Pople, J. A. *Chem. Phys. Lett.* **1993**, *209* (5), 506−512.
(35) Ray, K. B.; Hannon, J. B.; Plummer, E. W. *Chem. Phys. Lett.* **1990**, *171* (5), 469−474.
(36) Lai, Q.; Paskevicius, M.; Sheppard, D. A.; Buckley, C. E.; Thornton, A. W.; Hill, M. R.; Gu, Q.; Mao, J.; Huang, Z.; Liu, H. K.; Guo, Z.; Banerjee, A.; Chakraborty, S.; Ahuja, R.; Aguey-Zinsou, K.-F. *ChemSusChem* **2015**, *8* (17), 2789−2825.
(37) Bae, Y.-S.; Snurr, R. Q. *Microporous Mesoporous Mater.* **2010**, *132* (1−2), 300−303.
(38) Frost, H.; Snurr, R. Q. *J. Phys. Chem. C* **2007**, *111* (50), 18794−18803.
(39) Bhatia, S. K.; Myers, A. L. *Langmuir* **2006**, *22* (4), 1688−1700.
(40) Frost, H.; Düren, T.; Snurr, R. Q. *J. Phys. Chem. B* **2006**, *110* (19), 9565−9570.
(41) Savitzky, A.; Golay, M. J. E. *Anal. Chem.* **1964**, *36* (8), 1627.

DOI: 10.1021/jacs.6b00135
J. Am. Chem. Soc. 2016, 138, 3218−3227